Nano World Journal

https://doi.org/10.17756/nwj.2017-041

Research Article

Open Access

Hydrolysis of Hydrazine Borane for Chemical Hydrogen Storage by Highly Efficient Poly(*N*-vinyl-2-pyrrolidone)-protected Rhodium Nanoparticles

Bayram Abay[1], Nihat Tunç[1] and Murat Rakap[2*]

[1]*Department of Chemistry, Yuzuncu Yil University, 65080, Van, Turkey*
[2]*Maritime Faculty, Yuzuncu Yil University, 65080, Van, Turkey*

***Correspondence to:**
Murat Rakap, PhD
Department of Chemistry, Yuzuncu Yil University, 65080, Van, Turkey
Tel: 0090 432 225 17 01
Fax: 0090 432 486 54 13
E-mail: mrtrakap@gmail.com

Received: February 16, 2017
Accepted: April 19, 2017
Published: April 20, 2017

Citation: Abay B, Tunç N, Rakap M. 2017. Hydrolysis of Hydrazine Borane for Chemical Hydrogen Storage by Highly Efficient Poly(*N*-vinyl-2-pyrrolidone)-protected Rhodium Nanoparticles. *NanoWorld J* 3(1): 23-28.

Published by United Scientific Group

Abstract

The employment of poly(*N*-vinyl-2-pyrrolidone)-protected rhodium nanoparticles (3.8 ± 1.2 nm) as highly efficient catalysts in the hydrolysis of hydrazine borane for hydrogen generation is reported. The catalyst is prepared by reduction of rhodium metal ion in ethanol/water mixture by an alcohol reduction method and characterized by TEM analysis, UV-Vis spectroscopy, and X-ray photoelectron spectroscopy. It is durable and highly efficient catalysts for hydrogen generation from the hydrolysis of hydrazine borane even at very low concentrations and temperature, providing an average turnover frequency of 75 min^{-1}. Poly(*N*-vinyl-2-pyrrolidone)-protected rhodium nanoparticles also provide activation energy of 58.6 ± 2 kJ/mol for the hydrolysis of hydrazine borane.

Keywords

Rhodium, Nanoparticle, Hydrazine borane, Hydrogen, Hydrolysis

Introduction

Towards the safe and efficient hydrogen storage, chemical hydrogen storage is considered the most promising approach [1]. Among the various materials falling into this classification, lightweight boron compounds have received great attention due to their attractive properties of stability, high hydrogen density, safety, and environmentally benign side products [2]. Over the last 15 years, sodium borohydride and ammonia borane have widely been studied for this purpose [3]. Being one of those lightweight boron compounds, hydrazine borane ($N_2H_4BH_3$, HB) is a recently used promising hydrogen storage material. HB has a gravimetric hydrogen storage capacity of 15.4 wt %. HB efficiently releases hydrogen at room temperature in the presence of suitable catalysts via hydrolysis according to Equation 1:

$$N_2H_4BH_3(S) + 2H_2O(I) \xrightarrow[RT]{catalyst} N_2H_5^+(aq) + BO_2^-(aq) + 3H_2(g) \quad (1)$$

There are not so many catalysts employed for the hydrolysis of HB so far. The list of the tested catalysts includes only $Ni_{0.89}Pt_{0.11}$ nanoparticles [1], rhodium(III) chloride salt [4], hydroxyapatite-supported rhodium nanoparticles [5], nickel-based bimetallic nanocatalysts [6], rhodium-nickel catalysts [7], poly(4-styrenesulfonic acid-co-maleic acid)-stabilized nickel nanoparticles [8], supported Ni@(RhNi alloy) nanocomposites [9], nickel- and platinum-containing core-shell catalysts [10], surfactant-free nickel-platinum nanocatalysts [11], core-shell Cu@SiO_2 nanospheres [12], and poly(4-styrenesulfonic acid-co-maleic acid)-stabilized cobalt nanoparticles [13].

Herein, we report the first time use of highly efficient poly(*N*-vinyl-2-pyrrolidone)-protected rhodium nanoparticles (Rh@PVP NPs) in the hydrolysis of HB for hydrogen generation. PVP is a very versatile reagent that has been used for the preparation of nanocatalysts for hydrogen generation from boron containing compounds [14-17]. For the preparation of nanoparticles, PVP can be used as only stabilizer or both stabilizer and reducing agent as in our case. The catalyst has been prepared by the reduction of rhodium salt in the presence of PVP at reflux temperature. Rh@PVP NPs stable as colloidal dispersions are characterized by transmission electron microscopy (TEM), X-ray photoelectron spectroscopy (XPS), and UV-Vis spectroscopy. Although the cost of noble metal catalysts is assumed to be high, the highest catalytic activity of the Rh@PVP NPs makes them very promising candidates to be used as catalyst in developing efficient portable hydrogen generation systems using HB as solid hydrogen storage material since it would easily compensate the cost concerns.

Experimental Section

Materials

Rhodium(III) chloride trihydrate ($RhCl_3.3H_2O$), poly(*N*-vinyl-2-pyrrolidone) (PVP-40), hydrazine hemisulfate salt ($N_2H_4.0.5H_2SO_4$), sodium borohydride, and 1,4-dioxane were purchased from Aldrich. Ethanol was purchased from Merck. Deionized water was distilled by water purification system (Milli Q-pure WS). All glassware and teflon coated magnetic stir bars were rinsed with acetone, followed by copious washing with distilled water before drying in an oven at 150 °C.

Preparation of Rh@PVP nanoparticles

Rh@PVP nanoparticles were prepared by an alcohol reduction method in which PVP serves as both stabilizer and reducing agent [18, 19]. To a solution of rhodium(III) chloride trihydrate (0.25 mmol in 50 mL water/ethanol mixture), poly(*N*-vinyl-2-pyrrolidone) (PVP-40, 2.5 mmol of monomeric units) was added. Then, the resulting mixture was refluxed at 90 °C for 2 h. After refluxing for 2 h, the color of the solution turned to brownish black, indicating reduction of Rh^{3+} ion to Rh^0 to form nanoparticles. Monitoring the UV-Vis electronic absorption spectrum of the solution provides the best way to follow this conversion. Figure 1 shows the spectral change during the formation of Rh nanoparticles from the reduction of corresponding rhodium salt by PVP. The absorption band due to d-d transitions in Rh^{3+} ion completely disappear after refluxing the solution, indicating the complete reduction of corresponding ion.

Characterization of Rh@PVP nanoparticles

Transmission Electron Microscopy analysis was carried out using a JEOL-2010 microscope operating at 200 kV, fitted with a LaB6 filament and has lattice and theoretical point resolutions of 0.14 nm and 0.23 nm, respectively. Samples were examined at magnification between 100 and 400 K. One drop of dilute suspension of sample was deposited on the TEM grids and the solvent was then evaporated. The diameter of each particle was determined from the enlarged photographs. X-ray photoelectron spectrum of the nanoparticles was taken by using SPECS spectrometer equipped with a hemispherical analyzer and using monochromatic Mg-Kα radiation (1250 eV, the X-ray tube working at 15 kV and 350 W). UV-Vis spectra were recorded on a Cary 5000 (Varian) UV-Vis spectrophotometer. A quartz cell with a part length of 1 cm was used and spectra were collected over the range of 200-900 nm. ^{11}B NMR spectra were recorded on a Bruker Avance DPX 400 MHz spectrometer.

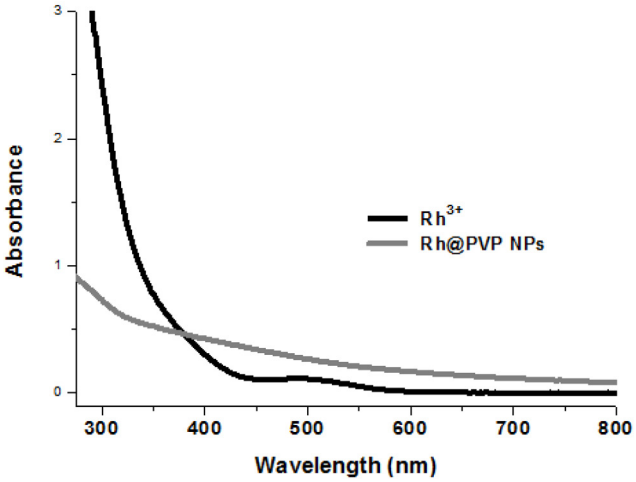

Figure 1: UV-Vis absorption spectra of the aqueous solutions of $RhCl_3{\cdot}3H_2O$ and Rh@PVP nanoparticles.

Synthesis and characterization of hydrazine borane ($N_2H_4BH_3$)

Hydrazine borane ($N_2H_4BH_3$) was synthesized from the reaction of hydrazine hemisulfate with sodium borohydride in 1,4-dioxane following the literature procedures [20, 21]. The melting point of hydrazine borane is ~ 60 °C. m/z = 46; ^1H NMR (400.1 MHz, CD_2Cl_2): 5.1 ppm (t, 2, NH_2-NH_2-BH_3), 3.4 ppm (b, 2, H_2N-NH_2-BH_3), 1.2 ppm (t, 3, H_2N-NH_2-BH_3); ^{11}B NMR (128.2 MHz, H_2O): -20 ppm (q, BH_3); ATR-IR: 3310 (s), 3200 (s), 2840 (m), 2650 (m), 2370 (m), 2214 (m), 1620 (s), 1588 (m), 1435 (w), 1332 (m), 1150 (s), 910 (m), 747 (w) in good agreement with the literature values [21].

Catalytic evaluation of Rh@PVP nanoparticles in the hydrolysis of HB

The catalytic activity of Rh@PVP nanoparticles in the hydrolysis of HB in aqueous solution was determined by measuring the rate of hydrogen generation. In all the experiments, a jacketed reaction flask (50 mL) containing a Teflon-coated stir bar was placed on a magnetic stirrer (Heidolph MR-301) and thermostated to 25.0 ± 0.1 °C by circulating water through its jacket from a constant temperature bath. Then, a graduated glass tube filled with water was connected to the reaction flask to measure the volume of the hydrogen gas to be evolved from the reaction. In a typical experiment, 46 mg (1 mmol) of $N_2H_4BH_3$ was dissolved in x mL of water. The solution was transferred with a glass pipet into the reaction flask thermostated at 25.0 ± 0.1 °C. Then, aliquots of Rh@PVP nanoparticles (10^{-x} mL) from

the stock solution (5.0 mM) were added into the reaction flask. The experiment was started by closing the flask and the volume of hydrogen gas evolved was measured by recording the displacement of water level at the stirring speed of 1000 rpm. In addition to the volumetric measurement of the hydrogen evolution, the conversion of HB (δ = -20 ppm, q) to hydrazinium metaborate (δ = 12.5 ppm, s) was also checked by ^{11}B NMR spectroscopy.

Kinetic studies for the hydrolysis of HB catalyzed by Rh@PVP nanoparticles

In order to establish the rate low for the hydrolysis of HB catalyzed by Rh@PVP nanoparticles, two different sets of experiments were carried out. In the first set of experiments, the concentration of $N_2H_4BH_3$ was kept constant at 100 mM and Rh@PVP nanoparticles concentration was varied in the range of 0.6, 0.8, 1.0, 1.2, and 1.4 mM. In the second set of experiments, Rh@PVP nanoparticles concentration was kept constant at 1.0 mM and $N_2H_4BH_3$ concentrations were varied in the range of 40, 60, 80, 100, and 120 mM.

Determination of activation energy of Rh@PVP nanoparticles in the hydrolysis of HB

In a typical experiment, the hydrolysis of $N_2H_4BH_3$ (100 mM) catalyzed by Rh@PVP nanoparticles (1.0 mM) was performed by following the same procedure described in Section 2.5. at various temperatures (15, 20, 25, 30, 35 °C). The values of observed rate constants (k_{obs}) for the catalytic hydrolysis of $N_2H_4BH_3$ were calculated from linear portions of each temperature and used to determine the activation energy (E_a).

Durability of Rh@PVP nanoparticles in the hydrolysis of HB

The durability of Rh@PVP nanoparticles in the hydrolysis of HB was determined by a series of experiments started with a 10 mL solution containing 1.0 mM Rh@PVP nanoparticles and 100 mM HB at 25.0 ± 0.1 °C. When the complete conversion is achieved, another equivalent of HB was added to the reaction mixture immediately. The results were expressed as % initial catalytic activity of Rh@PVP nanoparticles and % conversion of HB versus the number of catalytic runs in the hydrolysis of HB solution.

Results and Discussion

Characterization of Rh@PVP nanoparticles

The size, morphology and composition of Rh@PVP nanoparticles were investigated by TEM analysis. Figure 2 shows the TEM image taken at 20 nm magnification of Rh@PVP nanoparticles. The mean particle size was determined as 3.8 ± 1.2 nm from TEM image by counting 132 non-touching particles.

Figure 3 shows the survey scan (Figure 3A) XPS spectrum of Rh@PVP nanoparticles and high resolution XPS spectra of Rh 3d (Figure 3B) region. Rh 3d region shows two peaks observed at 306.2 eV for 3d5/2 and 310.9 eV for 3d3/2, confirming the presence of Rh(0) [22]. There is no higher oxidation state peaks for both metals of the catalyst in the XPS spectrum, indicating the protection of Rh(0) species by the attachment of PVP during catalyst preparation procedure.

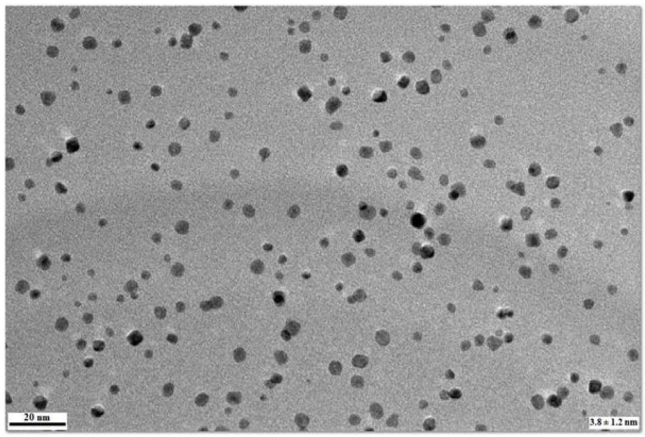

Figure 2: TEM image of Rh@PVP nanoparticles.

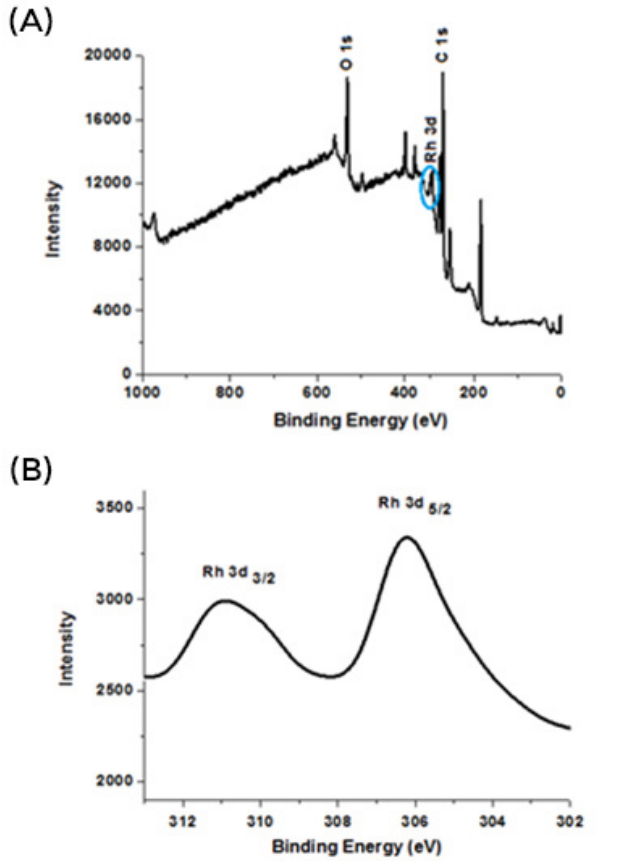

Figure 3: (A) Survey scan X-Ray photoelectron spectrum of Rh@PVP nanoparticles, **(B)** high resolution XPS spectrum of Rh 3d regions.

Catalytic activity of Rh@PVP nanoparticles in the hydrolysis of HB

Rh@PVP nanoparticles were found to be highly efficient catalyst for the hydrolysis of HB. Figure 4A shows the plot of mol H_2/mol HB versus time for the hydrolysis of 100 mM HB solutions in the presence of Rh@PVP nanoparticles in different catalyst concentrations at 25.0 ± 0.1 °C. The

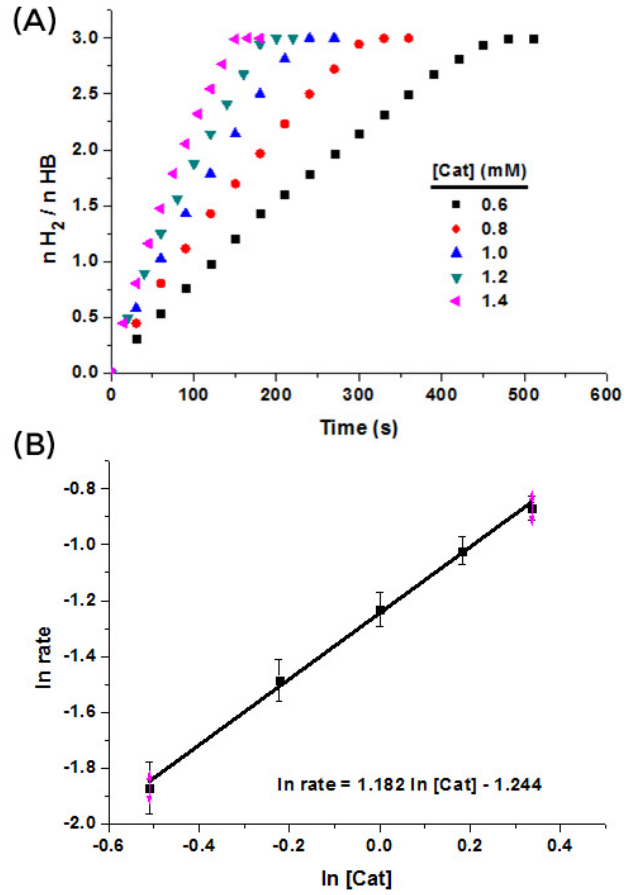

Figure 4: (A) Plots of mol H_2/mol HB versus time for the hydrolysis of 100 mM HB solutions in the presence of Rh@PVP nanoparticles at different catalyst concentrations (0.6, 0.8, 1.0, 1.2, and 1.4 mM) at 25.0 ± 0.1 °C. **(B)** Plot of the hydrogen generation rate versus the Rh@PVP nanoparticles catalyst concentration (both in logarithmic scale) for the hydrolysis of 100 mM HB at 25.0 ± 0.1 °C.

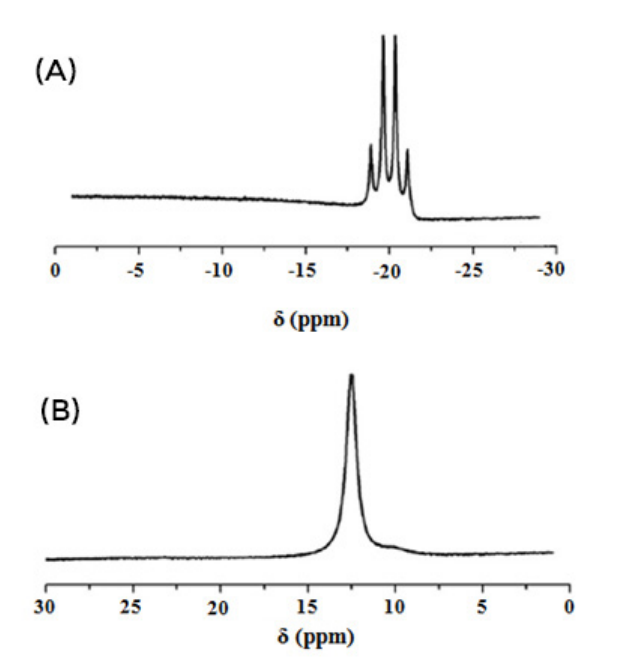

Figure 5: ^{11}B NMR spectrum **(A)** before and **(B)** after the hydrolysis of HB

linear hydrogen generation starts immediately without an induction period and continues until the complete hydrolysis of HB. Plotting the hydrogen generation rate, determined from the linear portion of plots in Figure 4A, versus catalyst concentration, both in logarithmic scales (Figure 4B), gives a straight line with a slope of 1.182 indicating that the hydrolysis of HB is first order with respect to the catalyst concentration. Additionally, the conversion of HB (δ = -20 ppm, q) to hydrazinium metaborate (δ = 12.5 ppm, s) was also checked by ^{11}B NMR spectroscopy (Figure 5).

The effect of $N_2H_4BH_3$ substrate concentration on the hydrolysis reaction was also studied by carrying out a series of experiments starting with various initial concentrations of HB while keeping Rh@PVP nanoparticles concentration constant at 1.0 mM. Figure 6A shows the plot of volume of generated hydrogen gas versus time for the hydrolysis of 100 mM HB solutions in the presence of Rh@PVP nanoparticles at different HB concentrations at 25.0 ± 0.1 °C. Plotting the hydrogen generation rate determined from the linear portion of plots in Figure 6A versus HB concentration, both in logarithmic scales (Figure 6B), gives a straight line with a slope of -0.094 indicating that the hydrolysis of HB is zero

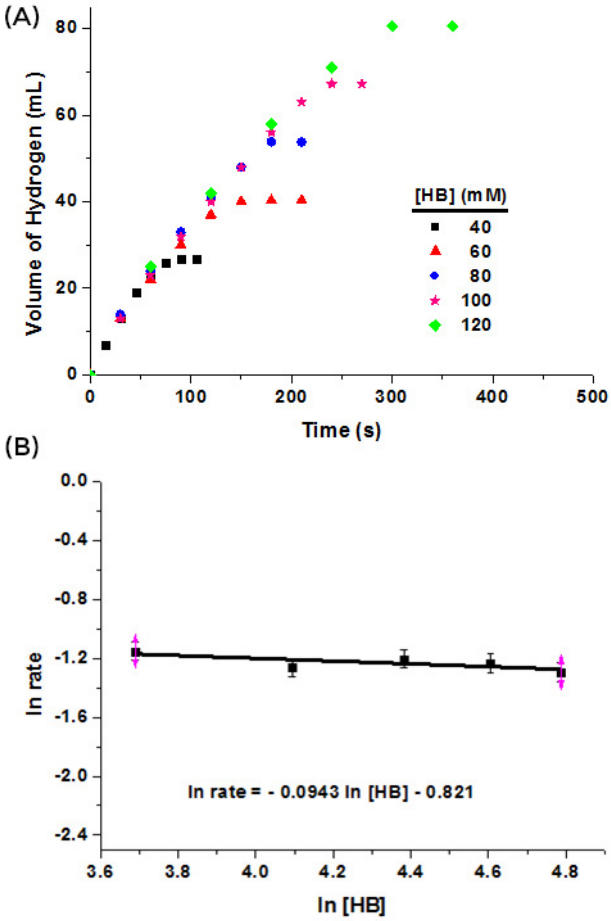

Figure 6: (A) Plots of volume of generated hydrogen gas versus time for the hydrolysis of HB in the presence of Rh@PVP nanoparticles (1.0 mM) at different HB concentrations (40, 60, 80, 100, and 120 mM) at 25.0 ± 0.1 °C. **(B)** Plot of the hydrogen generation rate versus HB concentration (both in logarithmic scale) for the hydrolysis of HB in the presence of Rh@PVP nanoparticles (1.0 mM) at 25.0 ± 0.1 °C.

order with respect to $N_2H_4BH_3$ concentration. Consequently, the rate law for the catalytic hydrolysis reaction of $N_2H_4BH_3$ can be given as in equation 2:

$$\frac{-3d\left[N_2H_4BH_3\right]}{dt} = \frac{d\left[H_2\right]}{dt} = k\left[catalyst\right] \quad \text{--------(2)}$$

The hydrolysis of HB catalyzed by Rh@PVP nanoparticles was also carried out at different temperatures to determine the activation energy. Figure 7 shows the plots mol H_2/mol HB versus time in the catalytic hydrolysis of 100 mM HB solutions in the presence of Rh@PVP nanoparticles (1.0 mM) at various temperatures (15, 20, 25, 30, 35 °C). It is worth to note that using Rh@PVP nanoparticles (1.0 mM) leads to complete hydrogen release (3.0 mol H_2/mol HB) for the hydrolysis of HB within 4 minutes, corresponding to an average TOF value of 75 min^{-1} at 25.0 ± 0.1 °C. This TOF value is much more higher than that of RhNi catalyst (1.5 min^{-1}) [8], poly(4-styrenesulfonic acid-co-maleic acid)-stabilized nickel nanoparticles (3.05 min^{-1}) [9], core-shell Cu@SiO_2 nanospheres (7.58 min^{-1}) [13], poly(4-styrenesulfonic acid-co-maleic acid)-stabilized cobalt nanoparticles (6.2 min^{-1}) [14], and poly(*N*-vinyl-2-pyrrolidone)-stabilized Pd nanoparticles (42.9 min^{-1}) [18].

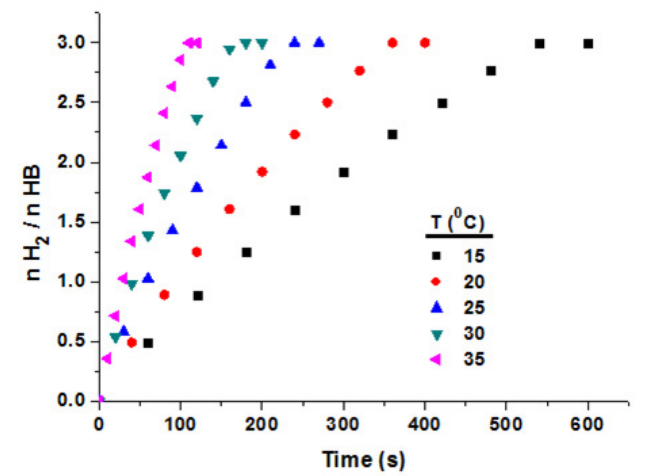

Figure 7: Plots of mol H_2/mol HB versus time in the catalytic hydrolysis of 100 mM HB solutions in the presence of Rh@PVP nanoparticles (1.0 mM) at various temperatures (15, 20, 25, 30, and 35 °C).

The rate constants of hydrogen generation from the hydrolysis of HB were calculated from the linear portions of the plots given in Figure 7 at five different temperatures and used for the calculation of the activation energy (E_a = 58.6 ± 2 kJ/mol) from the Arrhenius plot (Figure 8) for hydrolysis reaction. This activation energy of 58.6 ± 2 kJ/mol for the hydrolysis of HB is lower than that of poly(4-styrenesulfonic acid-co-maleic acid)-stabilized nickel nanoparticles (73 ± 2 kJ/mol) [9] and poly(4-styrenesulfonic acid-co-maleic acid)-stabilized cobalt nanoparticles (60 ± 2 kJ/mol) [14], but higher than that of rhodium(III) chloride (44 ± 2 kJ/mol) [5] and hydroxyapatite-supported rhodium nanoparticles (45 ± 2 kJ/mol) [6].

The durability of Rh@PVP nanoparticles in the hydrolysis of HB

The durability of Rh@PVP nanoparticles in the hydrolysis of HB was investigated by successive additions of HB after the first cycle of the hydrolysis reaction. The Rh@PVP nanoparticles catalyst retains 73% of its initial catalytic activity in the hydrolysis of HB, even at the sixth run (Figure 9). The slight decrease in the catalytic activity of Rh@PVP nanoparticles is most probably due to the passivation of nanoparticles' surface by increasing amount of metaborate, which decreases accessibility of active sites [23] and the aggregation of nanoparticles.

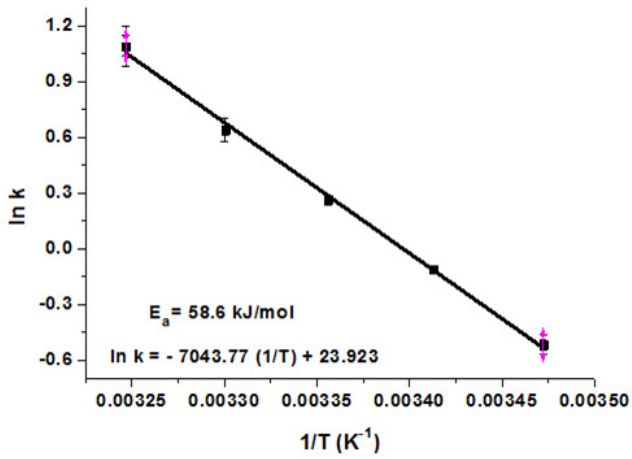

Figure 8: Arrhenius plot for the hydrolysis of HB (100 mM) catalyzed by 1.0 mM Rh@PVP nanoparticles.

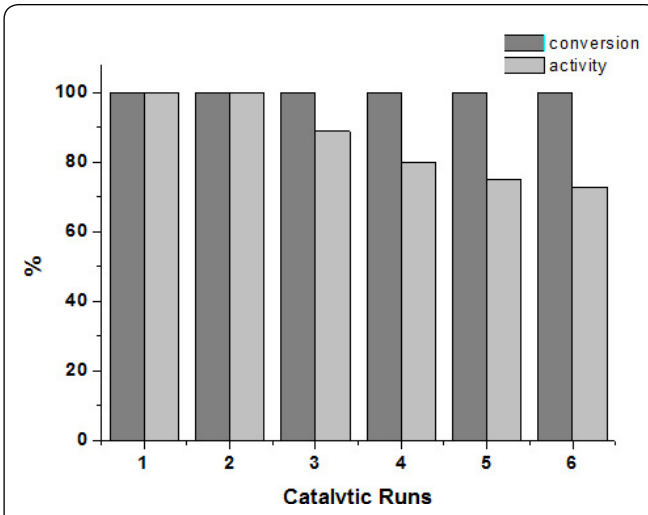

Figure 9: % Conversion of HB and retained % catalytic activity of Rh@PVP nanoparticles (1.0 mM) in the successive catalytic runs for the hydrolysis of 100 mM HB at 25.0 ± 0.1 °C.

Conclusions

In summary, this study of the preparation, characterization and employment of Rh@PVP nanoparticles as catalyst for the hydrolysis of HB has led to the following conclusions and insights:

Rh@PVP nanoparticles can be easily prepared from the reduction of corresponding rhodium salt by an alcohol reduction method.

Rh@PVP nanoparticles are found to be highly efficient

catalyst for hydrogen generation from the hydrolysis of HB.

They provide an average TOF value of 75 min^{-1} for the hydrolysis of HB.

Activation energy for the catalytic hydrolysis of HB in the presence of Rh@PVP nanoparticles was determined as 58.6 ± 2 kJ/mol.

Rh@PVP nanoparticles can be regarded as promising catalysts with a high catalytic activity for practical applications to supply hydrogen from the hydrolysis of HB for proton exchange membrane fuel cells.

Acknowledgements

The TEM and XPS analyses were carried out at the Central Laboratory of Middle East Technical University in Ankara.

References

1. Hannauer J, Akdim O, Demirci UB, Geantet C, Herrmann JM, et al. 2011. High-extent dehydrogenation of hydrazine borane $N_2H_4BH_3$ by hydrolysis of BH_3 and decomposition of N_2H_4. *Energy Environ Sci* 4(9): 3355-3358. https://doi.org/10.1039/C1EE01886H
2. Hamilton CW, Baker RT, Staubitz A, Manners I. 2009. B-N compounds for chemical hydrogen storage. *Chem Soc Rev* 38(1): 279-293. https://doi.org/10.1039/b800312m
3. Chandra M, Xu Q. 2006. A high-performance hydrogen generation system: transition metal-catalyzed dissociation and hydrolysis of ammonia-borane. *J Power Sources* 156(2): 190-194. https://doi.org/10.1016/j.jpowsour.2005.05.043
4. Karahan S, Zahmakıran M, Özkar S. 2011. Catalytic hydrolysis of hydrazine borane for chemical hydrogen storage: highly efficient and fast hydrogen generation system at room temperature. *Int J Hydrogen Energy* 36(8): 4958-4966. https://doi.org/10.1016/j.ijhydene.2010.12.129
5. Çelik D, Karahan S, Zahmakıran M, Özkar S. 2012. Hydrogen generation from the hydrolysis of hydrazine-borane catalyzed by rhodium(0) nanoparticles supported on hydroxyapatite. *Int J Hydrogen Energy* 37(6): 5143-5151. https://doi.org/10.1016/j.ijhydene.2011.12.067
6. Çakanyıldırım Ç, Demirci UB, Şener T, Xu Q, Miele P. 2012. Nickel-based bimetallic nanocatalysts in high-extent dehydrogenation of hydrazine borane. *Int J Hydrogen Energy* 37(12): 9722-9729. https://doi.org/10.1016/j.ijhydene.2012.03.054
7. Zhong DC, Aranishi K, Singh AK, Demirci UB, Xu Q. 2012. The synergistic effect of Rh-Ni catalysts on the highly-efficient dehydrogenation of aqueous hydrazine borane for chemical hydrogen storage. *Chem Commun(Camb)* 48(98): 11945-11947. https://doi.org/10.1039/C2CC36407G
8. Şencanlı S, Karahan S, Özkar S. 2013. Poly(4-styrenesulfonic acid-co-maleic acid) stabilized nickel(0) nanoparticles: highly active and cost effective catalyst in hydrogen generation from the hydrolysis of hydrazine borane. *Int J Hydrogen Energy* 38(34): 14693-14703. https://doi.org/10.1016/j.ijhydene.2013.09.060
9. Li C, Dou Y, Liu J, Chen Y, He S, et al. 2013. Synthesis of supported Ni@(RhNi-alloy) nanocomposites as an efficient catalyst towards hydrogen generation from $N_2H_4BH_3$. *Chem Commun (Camb)* 49(85): 9992-9994. https://doi.org/10.1039/c3cc45697h
10. Clemençon D, Petit JF, Demirci UB, Xu Q, Miele P. 2014. Nickel- and platinum-containing core@shell catalysts for hydrogen generation of aqueous hydrazine borane. *J Power Sources* 260: 77-81. https://doi.org/10.1016/j.jpowsour.2014.03.015
11. Zhu QL, Zhong DC, Demirci UB, Xu Q. 2014. Controlled synthesis of ultrafine surfactant-free NiPt nanocatalysts toward efficient and complete hydrogen generation from hydrazine borane at room temperature. *ACS Catal* 4(12): 4261-4268. https://doi.org/10.1021/cs501329c
12. Yao Q, Lu ZH, Zhang Z, Chen X, Lan Y. 2014. One-pot synthesis of core-shell Cu@SiO_2 nanospheres and their catalysis for hydrolytic dehydrogenation of ammonia borane and hydrazine borane. *Sci Rep* 4: 7597. https://doi.org/10.1038/srep07597
13. Karahan S, Özkar S. 2015. Poly(4-styrenesulfonic acid-co-maleic acid) stabilized cobalt(0) nanoparticles: a cost-effective and magnetically recoverable catalyst in hydrogen generation from the hydrolysis of hydrazine borane. *Int J Hydrogen Energy* 40(5): 2255-2265. https://doi.org/10.1016/j.ijhydene.2014.12.028
14. Rakap M. 2014. Hydrogen generation from hydrolysis of ammonia borane in the presence of highly efficient poly(*N*-vinyl-2-pyrrolidone)-protected platinum-ruthenium nanoparticles. *Appl Catal A: Gen* 478: 15-20. https://doi.org/10.1016/j.apcata.2014.03.022
15. Rakap M. 2015. The highest catalytic activity in the hydrolysis of ammonia borane by poly(*N*-vinyl-2-pyrrolidone)-protected palladium-rhodium nanoparticles for hydrogen generation. *Appl Catal B: Env* 163: 129-134. https://doi.org/10.1016/j.apcatb.2014.07.050
16. Rakap M. 2015. Poly(*N*-vinyl-2-pyrrolidone)-stabilized palladium-platinum nanoparticles-catalyzed hydrolysis of ammonia borane for hydrogen generation. *J Power Sources* 276: 320-327. https://doi.org/10.1016/j.jpowsour.2014.11.146
17. Rakap M. 2015. Hydrogen generation from hydrolytic dehydrogenation of hydrazine borane by poly(*N*-vinyl-2-pyrrolidone)-stabilized palladium nanoparticles. *J Power Sources* 299: 403-407. https://doi.org/10.1016/j.jpowsour.2015.09.032
18. Rakap M. 2015. PVP-stabilized Ru-Rh nanoparticles as highly efficient catalysts for hydrogen generation from hydrolysis of ammonia borane. *J Alloy Compd* 649: 1025-1030. https://doi.org/10.1016/j.jallcom.2015.07.249
19. Gniewek A, Trzeciak AM. 2013. Rh(0) Nanoparticles: Synthesis, structure and catalytic application in Suzuki-Miyaura reaction and hydrogenation of benzene. *Top Catal* 56(13): 1239-1245. https://doi.org/10.1007/s11244-013-0090-6
20. Moury R, Moussa G, Demirci UB, Hannauer J, Bernard S, et al. 2012. Hydrazine borane: synthesis, characterization, and application prospects in chemical hydrogen storage. *Phys Chem Chem Phys* 14(5): 1768-1777. https://doi.org/10.1039/C2CP23403C
21. Gunderloy Jr. FC, Spielvogel B, Parry RW. 1967. Hydrazine-mono- and -bisborane. In: Tyree SY (ed) Inorganic syntheses, volume 9. John Wiley & Sons, Inc., Hoboken, NJ, USA, pp 13-16. https://doi.org/10.1002/9780470132401.ch5
22. Durap F, Zahmakıran M, Özkar S. 2009. Water soluble laurate-stabilized rhodium(0) nanoclusters catalyst with unprecedented catalytic lifetime in the hydrolytic dehydrogenation of ammonia-borane. *Appl Catal A: Gen* 369(1-2): 53-59. https://doi.org/10.1016/j.apcata.2009.08.031
23. Clark TJ, Whittell GR, Manners I. 2007. Highly efficient colloidal cobalt- and rhodium-catalyzed hydrolysis of $H_3N.BH_3$ in air. *Inorg Chem* 46(18): 7522-7527. https://doi.org/10.1021/ic700806b